

# Cohesive zone modeling of fracture in irregular lattices

J.E. Bolander

*Department of Civil & Environmental Engineering, Univ. of California, Davis, California, USA*

S. Berton

*Department of Civil Engineering, Kyushu University, Fukuoka, Japan*

**ABSTRACT:** This paper describes a cohesive zone modeling of fracture in three-dimensional irregular lattices. Lattice geometry is based on a Voronoi discretization of the material domain. In addition to being an effective means for discretization, the Voronoi diagram provides scaling rules for the elemental stiffness relations and fracture criteria. The lattice model provides an elastically uniform representation of the material. The cohesive zone representation of fracture is implemented using a crack band approach and is objective with respect to the irregular geometry of the lattice. Model performance is demonstrated through simulated fracture testing of a notched concrete beam.

**Keywords:** irregular lattice, crack band model, concrete fracture, cohesive zone, rigid-body-spring network

## 1 INTRODUCTION

Lattice models have been used to study fracture in a variety of materials, including concrete (Schlangen & van Mier 1992, Schlangen & Garboczi 1997, Cusatis et al. 2001, Lilliu & van Mier 2003). A lattice model is a collection of simple one-dimensional elements that interconnect at lattice sites, which are regularly or irregularly positioned in space. The computational degrees of freedom are defined at the lattice sites (or nodes). The lattice modeling of concrete materials is attractive, due to the discrete structure of the lattice. However, discrete networks have difficulty modeling some basic aspects of homogeneous systems, such as their elastic uniformity during uniform straining (Schlangen & Garboczi 1997). Regular lattice models generally satisfy this requirement due to site symmetry of the lattice. Irregular lattice models generally exhibit artificial heterogeneity, which has strong implications toward their ability to model fracture.

Based on the concept of a rigid-body-spring model (Kawai 1978), elastically uniform irregular lattices have been developed and applied to modeling structural concrete (Bolander & Saito 1998, Bolander et al. 2001, Bolander & Hong 2002). A key feature of this lattice model, which separates it from an ordinary rigid-body-spring

model, is the scaling of the elemental stiffness and fracture properties according to a Voronoi discretization of the material domain. A crack band modeling of fracture (Bazant & Oh 1983) conserves fracture energy and is objective for mode I type openings within irregular lattices. When modeling cracking in homogeneous phases of materials, fracture localizes into the narrowest band permitted by the mesh size and, therefore, the model can be regarded as a cohesive zone representation of fracture. The previous references to this Rigid-Body-Spring Network (RBSN) approach have been for planar analyses. This paper describes the extension of the RBSN fracture models to three-dimensions, with an application to modeling fracture of a concrete beam specimen.

## 2 MODEL CONSTRUCTION

### *2.1 Domain discretization*

As noted in the introduction, the RBSN is defined by a Voronoi discretization of the material domain based on an irregular set of points, which serve as computational nodes. Discretization starts with the specification of coordinates for the bounding box that encloses the three-dimensional domain (Fig. 1). Thereafter, the following steps are taken during the discretization process:

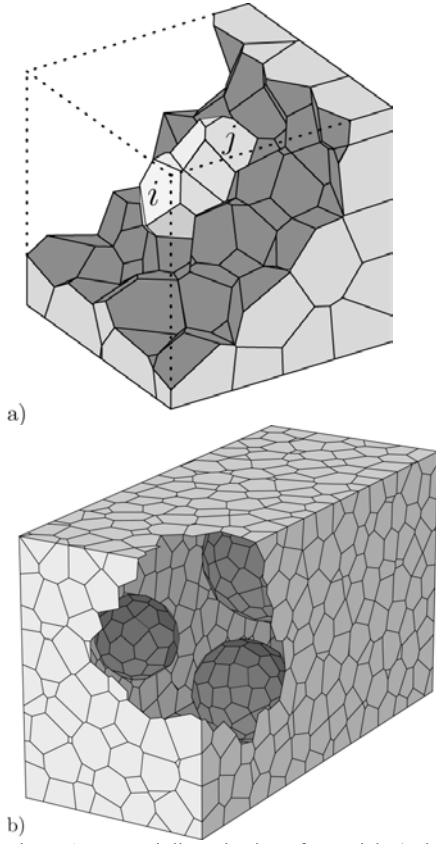


Figure 1. Voronoi discretization of material: a) element  $ij$  within a cubic domain; and b) domain with spherical inclusions.

- quasi-random insertion of points until the three-dimensional domain is saturated with such points (i.e. computational nodes);
- placement of an auxiliary point set related to boundary construction (Bolander & Saito 1998); and
- construction of the Voronoi tessellation (Sugihara et al. 1985) of the complete point set.

By strategically introducing interior and auxiliary points, various other geometries can be discretized, including domains with inclusions (Fig. 1b) and non-convex domains. There are a number of procedures for constructing the Voronoi diagram directly from the generated point set. Here, the Voronoi diagram is constructed from its dual, the Delaunay tessellation, since the latter is generally easier to construct and a robust program was available for doing so (Taniguchi et al. 2002).

## 2.2 Elastic material relations

Each pair of contiguous Voronoi cells forms a lattice element, as shown in Figure 1a and in detail

in Figure 2. The element is composed of a zero-size spring set, located at the area centroid (point C) of the Voronoi facet common to nodes  $i$  and  $j$ , and rigid arm constraints that link the spring set with the nodal degrees of freedom. The spring set consists of three lineal springs, oriented normal and tangential to the facet, and three rotational springs about the same local axes. This notion of a rigid-body-spring model was developed by Kawai (1978) and refined through Voronoi scaling of the spring constants (Bolander & Saito 1998, Bolander et al. 2001). For the lineal springs:

$$k_x = k_y = k_z = E \frac{A_{ij}}{h_{ij}} \quad (1)$$

and for the rotational springs:

$$k_{\phi_x} = E \frac{J_p}{h_{ij}}, \quad k_{\phi_y} = E \frac{I_{11}}{h_{ij}}, \quad k_{\phi_z} = E \frac{I_{22}}{h_{ij}} \quad (2)$$

where  $A_{ij}$  is the facet area;  $h_{ij}$  is the element length (i.e. the distance between  $i$  and  $j$ );  $E$  is the elastic modulus;  $J_p$  is the polar moment of inertia; and  $I_{11}$  and  $I_{22}$  are the two principal moments of inertia of the facet area. Berton (2003) provides additional details of the three-dimensional RBSN formulation. Although the approach is unconventional, the elemental stiffness relations are similar to those of an ordinary beam-column element. For this reason, and others, we categorize the approach as a lattice model. By virtue of the Voronoi scaling of the spring constants (Eq. 1), the lattice is elastically uniform during uniform straining (Bolander & Saito 1998, Bolander et al. 2001).

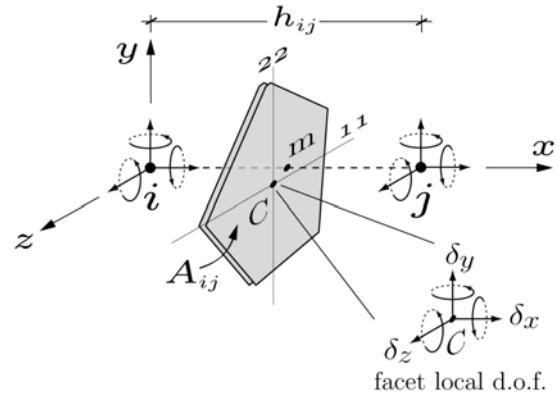


Figure 2. Basic element  $ij$  of the Rigid-Body-Spring Network.

## 2.3 Fracture criteria

The RBSN modeling of fracture is based on the crack band concept (Bazant & Oh 1983). Previous applications of the RBSN fracture model have been limited to planar analyses (Bolander et al. 2001, Bolander & Hong 2002). To discuss the three-

dimensional fracture formulation, consider an element formed by cells  $i$  and  $j$ , as described in the previous section (Fig. 2). In general, loading of an element will be skew to the element axis  $ij$  and the cells tend to separate accordingly; the normal and tangential springs are activated with the normal spring in tension (Fig. 3a). The fracture criterion is based on a measure of stress  $\sigma_R$ , which is defined as:

$$\sigma_R = \frac{F_R}{A_{ij}^p} \quad (3)$$

where  $F_R$  is the resultant force acting on the element facet and  $A_{ij}^p$  is the projection of the facet area on a plane perpendicular to the direction of the resultant (Fig. 3a). At every step of the simulation, the ratio  $\sigma_R/\sigma(w)$  is computed for all of the elements. Here, the cohesive stress  $\sigma(w)$  is a bilinear function of the crack opening displacement  $w$  (Fig. 4). For the element with  $\max(\sigma_R/\sigma(w)) > 1$ , a prismatic crack zone initiates (or continues to develop) within the element as shown in Figure 3b.

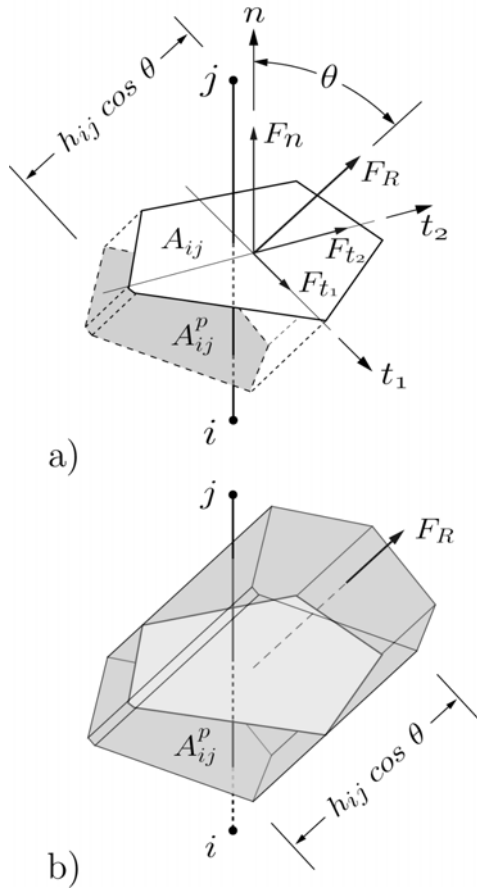


Figure 3. a) Resultant force on element facet; and b) elemental crack band volume.

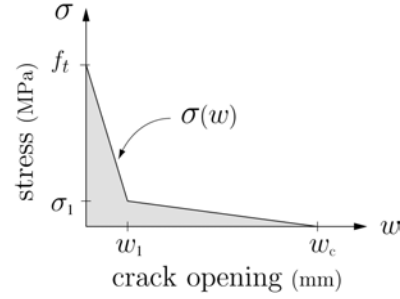


Figure 4. Bilinear softening relation.

The width of this zone (which corresponds to crack band width in the two-dimensional case) is  $h_{ij} \cos \theta$ , where  $\theta$  is the angle that the resultant force  $F_R$  forms with the normal to the facet. Crack opening displacement  $w$  is related to the fracture strain  $\epsilon_R$  over the crack zone:

$$\epsilon_R = \frac{w}{h \cos \theta} \quad (4)$$

For a critical element, fracture involves an isotropic reduction of the spring stiffnesses and an associated release of spring forces, so that  $\sigma_R$  follows the material softening relation. The release of spring forces causes an imbalance between the external and internal nodal force vectors, which is corrected through conventional equilibrium iterations. A maximum of one element spring set is modified per iteration cycle. While this approach is computationally demanding, it is stable in that zero-energy modes of deformation do not occur.

### 3 BEND TEST SIMULATION

The ability of the three-dimensional RBSN to represent a uniform strain field has been demonstrated elsewhere (Bolander et al. 2001). Here, a three-point bend test of a notched concrete beam is simulated to show the fracture properties of the irregular lattice network. The beam test was part of a series of round robin tests, which were performed to evaluate a method for determining the tension softening properties of concrete (Kitsutaka et al. 2001).

#### 3.1 Test specimen

Figure 5 shows a Voronoi discretization of the typical configuration for the test series. Here, the batch C test carried out at Gifu University is used for the comparison (Kitsutaka et al. 2001). The characteristics of the concrete are as follows:  $f_c = 40.9$  MPa;  $f_t = 3.46$  MPa;  $E = 31.6$  GPa; slump = 6.3 cm; and air content = 3.4%. The dimensions of the specimen are 100 x 100 x 400 mm with a span

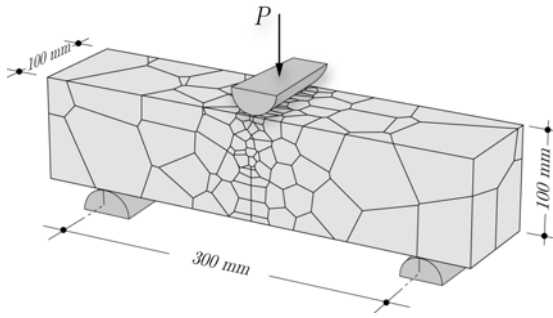


Figure 5. Voronoi discretization of three-point bend test.

of 300 mm. The notch has a depth of half the height of the beam (50 mm).

### 3.2 Softening parameters through inverse analysis

The four parameters defining the bilinear softening relation (Fig. 4) were determined using an inverse analysis procedure, based on a Levenberg-Marquardt minimization algorithm (Thomure et al. 2001). Starting with an assumed softening curve, the softening curve parameters are gradually adjusted to reduce the error between each successive computed load-CMOD curve and the experimental load-CMOD curve. To speed up this process, a planar RBSN model of the three-point bend test was used for the inverse analyses. Based on the experimental load-CMOD curve shown in Figure 6, the inverse procedure gave the following values for the softening parameters:  $f_t = 4.119$  MPa,  $\sigma_f = 1.018$  MPa,  $w_f = 0.0182$  mm and  $w_c = 0.1540$  mm.

### 3.3 Model description

Two different meshes are used to model the three-point bend test of the notched-beam specimen. The models are similar in terms of number of nodes and elements. However, a different approach has been used to discretize the ligament zone above the notch. In the first model, shown in Figure 5, a random procedure has been employed to generate the entire mesh. For the other case, a semi-random discretization is used, such that a predefined planar surface is created above the notch. Because of the imposed load applied to the specimen during the simulated test, the crack is likely to develop and propagate along this predefined flat surface. During the generation of both meshes, several nodes were prepositioned to accurately model the locations for supports and imposing displacements. The prenotch was modeled by assigning zero stiffness values to the elements crossing the prenotch area.

### 3.4 Simulation results

The analyses are carried out by imposing, in small increments, a downward displacement at the top mid-span nodes to simulate the action of the loading device (Fig. 5). For each mesh type described above, the resulting load-CMOD curves and fracture energy distributions are compared with experiment and theory in the following sections.

#### 3.4.1 Load-CMOD response

Figure 6 compares the load-CMOD curves obtained from the simulations with the experimental curve. The two simulated curves agree well with the experimental result. The higher load capacity of the numerical models in the tail region of the curves is due to the rather coarse discretization of the ligament region. The uppermost elements in that region remain in compression and therefore limit the advance of the fracture process zone. A forward analysis using the planar RBSN model (used for the inverse analysis in section 3.2) provides a better fit over the length of the curve, partly due to a finer discretization of the ligament region.

#### 3.4.2 Distribution of fracture energy density

At each step of the numerical simulation, the energy consumed by a fracturing element can be derived as the difference between the work done by the external loads and the internal strain energy. Since only one element is allowed to fracture during each computational cycle, the difference between the incremental values of external work and strain energy must be equal to the energy consumed by that critical element. Therefore, at any stage during the numerical simulation, the total energy consumed by one element can be determined by summing all its contributions up to that point. By dividing this energy by the projected area of the element facet on the cracking plane, the corresponding energy density is calculated. If an

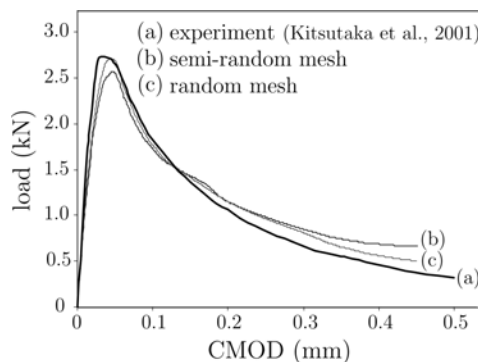


Figure 6. Load-CMOD response.

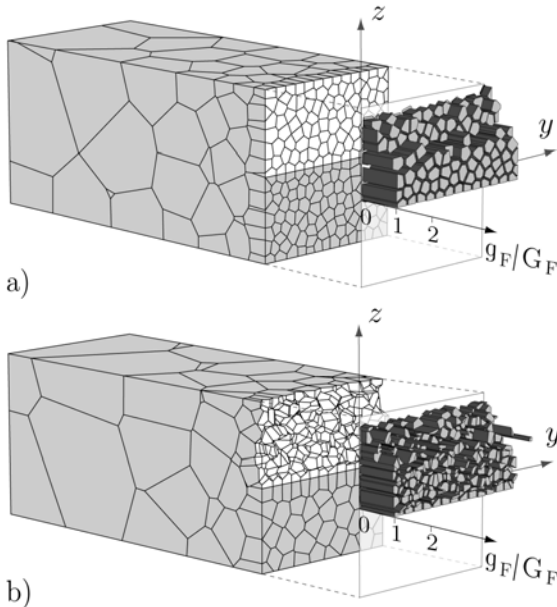


Figure 7. Normalized energy consumption for: a) semi-random and b) random discretization of ligament length.

element fractures completely (i.e.  $w > w_c$ ), the total energy consumed by that element should be equal to the fracture energy  $G_F$ , which is the area under the softening curve given in Figure 4.

Figures 7a and 8a show plots of the energy consumed by the fractured elements for the semi-random mesh simulation. The three-dimensional representations of the energy consumption are plotted alongside the cracked surface on the corresponding mesh view. Here, the local energy consumption,  $g_F$ , is normalized with respect to the fracture energy  $G_F = 115.9$  N/m, calculated from the bilinear softening relation shown in Figure 4. The lateral view of the plot shows that  $g_F/G_F$  is approximately equal to unity for the fully fractured elements (i.e. the elements located in the bottom part of the ligament zone). For these elements, the differences between  $g_F$  and  $G_F$  are within 1.9%. In the upper part of the ligament, the values of energy consumption decrease since the elements in that location have only partially fractured prior to reaching the final CMOD value of 0.45 mm (Fig. 6).

Figures 7b and 8b show plots of the fracture energy density obtained from the random mesh simulation. The profile of the energy density plot exhibits more variation relative to that of the semi-random mesh model due, in part, to the various facet inclinations with respect to the vertical plane. (In the figures, the values of the energy density are plotted only for elements with  $A_{ij}^p > 0.1$  mm<sup>2</sup> and angle  $\theta$  smaller than 70 degrees.) Although the

maximum value of the normalized energy density is about 45% larger than  $G_F$ , the average value for the fully fractured elements is 118.6 N/m, which is only 2.3% greater than  $G_F$ . As for the semi-random mesh case, the normalized energy consumption is fairly uniform and around unity for the elements in the lower part of the ligament. The energy values decrease in the upper part where the elements have not completely fractured by the end of the loading history.

#### 4 CONCLUSION

There are significant advantages to the irregular discretization of materials and structures, including the potential for highly automated model construction, effective gradations of nodal point density, and the explicit representation of material features. In general, however, irregular lattice models exhibit artificial heterogeneity that strongly affects their accuracy when simulating fracture.

The Rigid-Body-Spring Network (RBSN) approach is elastically homogeneous during uniform straining, by virtue of the Voronoi scaling of the lattice geometry and elemental stiffness coefficients. A cohesive zone representation of fracture was implemented in the RBSN using the crack band concept of Bazant & Oh (1983). This paper describes the extension of the RBSN fracture routines to three dimensions. Accuracy of the fracture model is demonstrated through simulations of a three-point bend test. The analysis results indicate that the RBSN modeling of mode I type fracture is objective with respect to irregular mesh geometry. Current work involves the explicit modeling of heterogeneous features, including fibers, in the concrete and the development of efficient strategies for solving larger systems.

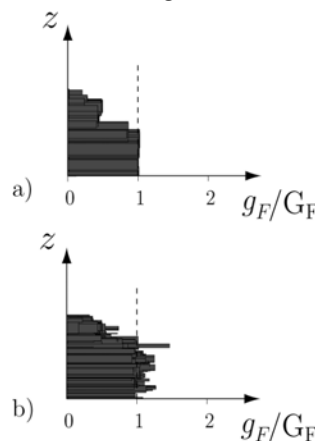


Figure 8. Normalized energy consumption for: a) semi-random and b) random discretization of the ligament length.

## ACKNOWLEDGEMENTS

This work is part of an ongoing research project on modeling overlay systems made of fiber-reinforced cement composites, supported by the US National Science Foundation through grant (CMS-0201590) to the University of California at Davis. The authors would also like to thank Mien Yip for his assistance in several aspects of this work.

## REFERENCES

- Bazant, Z.P. & Oh, B.H. 1983. Crack band theory for fracture of concrete. *Materials and structures*, RILEM, 16(93):155-177.
- Berton, S. (2003) Numerical simulation of the durability mechanics of cement-based materials, Ph.D. thesis, Civil and Environmental Engineering, University of California, Davis.
- Bolander, J.E. & Hong, G.S. 2002. Rigid-Body-Spring-Network modeling of prestressed concrete members. *ACI Structural Journal* 99(5): 595-604
- Bolander, J.E., Moriizumi, K., Kunieda, M., & Yip, M. 2001. Rigid-Body-Spring Network modeling of cement-based composites. In R. de Borst et al. (eds.), *Fracture Mechanics of Concrete Structures*. Lisse: Swets & Zeitlinger, 773-780.
- Bolander, J.E. & Saito, S. 1998. Fracture analysis using spring networks with random geometry. *Engng Fracture Mech* 61: 569-591.
- Cusatis, G., Bazant, Z.P. & Cedolin, L. 2001. 3D lattice model for dynamic simulations of creep, fracturing and rate effect in concrete. In F.-J. Ulm et al. (eds.), *Creep, shrinkage and durability mechanics of concrete and other quasi-brittle materials*. Oxford: Elsevier Science Ltd, 113-118.
- Kawai, T. 1978. New discrete models and their application to seismic response analysis of structures. *Nuclear Engineering and Design* 48: 207-229.
- Kitsutaka, Y., Uchida, Y., Mihashi, H., Kaneko, Y., Nakamura, S. & Kurihara, N. 2001. Draft on the JCI standard test method for determining tension softening properties of concrete. In R. de Borst et al. (eds.), *Fracture Mechanics of Concrete Structures*. Lisse: Swets & Zeitlinger, 371-376.
- Lilliu, G. & van Mier, J.G.M. 2003. 3D lattice type fracture model for concrete. *Engineering Fracture Mechanics* 70: 927-941.
- Okabe, A., Boots, B. & Sugihara, K. 1992. *Spatial tessellations: concepts and applications of Voronoi diagrams*. London: John Wiley & Sons Ltd.
- Schlangen, E. & Garboczi, E.J. 1997. Fracture simulations of concrete using lattice models: computational aspects. *Engineering Fracture Mechanics* 57(2/3): 319-332.
- Schlangen, E. & van Mier, J.G.M. 1992. Experimental and numerical analysis of micromechanisms of fracture of cement-based composites. *Cem. Conc. Composites* 14: 105-118.
- Taniguchi, T., Yamashita, Y. & Moriwaki, K. 2002. Generation of arbitrary 3-dimensional domain from nodes on its surface. *8th Conference on Numerical Grid Generation, Hawaii, USA, June 2002*.
- Thomure, J.L., Bolander, J.E. & Kunieda, M. 2001. Reducing mesh bias on fracture within Rigid-Body-Spring-Networks. *JSCE Structural Engineering/Earthquake Engineering* (18)2: 95-103.